Scanning Electron Microscopy

11-3-1984

Advances in Non-Contact Thermal-Wave Imaging with Infrared Detection

F. H. Dacol
IMB T.J. Watson Research Center

H. Ermert
Universität Erlangen-Nürnberg

R. L. Melcher
IBM T.J. Watson Research Center

Follow this and additional works at: https://digitalcommons.usu.edu/electron

Part of the Biology Commons

Utah State University
MERRILL-CAZIER LIBRARY

ADVANCES IN NON-CONTACT THERMAL-WAVE IMAGING WITH INFRARED DETECTION

F. H. Dacol*, H. Ermert[a] and R. L. Melcher

IBM T. J. Watson Research Center, P. O. Box 218, Yorktown Heights, NY 10598 USA
[a]Permanent address: Institut für Hochfrequenztechnik, Universität Erlangen-Nürnberg, Cauerstr. 9, 8520 Erlangen, West Germany

Abstract

We are making further advances in non-destructive and non-contact thermal imaging with infrared detection. We employ a chopped and scanned electron beam as heat source, a cooled HgCdTe infrared detector as temperature sensor, and digital processing of the measured temperature pattern for display and storage. The results give a convincing, high contrast image of subsurface structures.

Introduction

There is increasing interest in non-contact and non-destructive thermal imaging of subsurface inhomogeneities. [1-6,8,10-14]. Generation of a surface thermal wave can be accomplished with a scanned and modulated energy beam, for example, an electron or laser beam. Such surface thermal waves can be efficiently detected with proper non-contact optics and suitable infrared detectors.[5,12] In this paper, we report further progress on the detection of subsurface inhomogeneities through the emitted infrared radiation generated as a result of surface heating.[7] This technique responds to thermal waves only and its detection system has no contact with the sample.[9]

Experiment

The energy source of our thermal imaging system consists of a scanning electron microscope, Cambridge Mark II A. The chopped electron beam scans the sample in discrete steps and heats those points for a specific time, as shown in Fig. 1. The sample used in this study consists

*Address for correspondence: IBM Thomas J. Watson Research Center, P. O. Box 218, Yorktown Heights, NY 10598 USA Phone (914) 945-2335
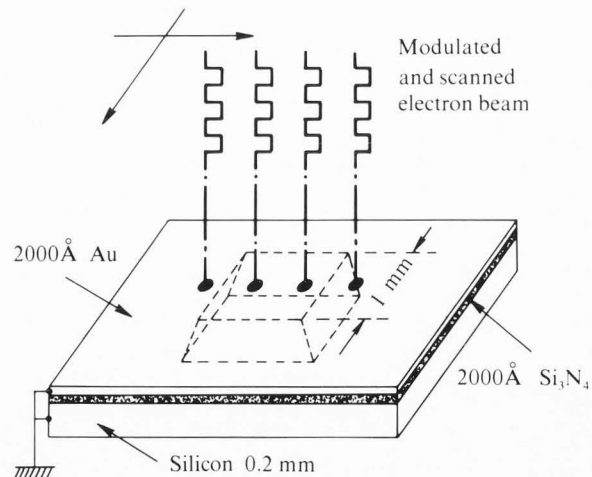
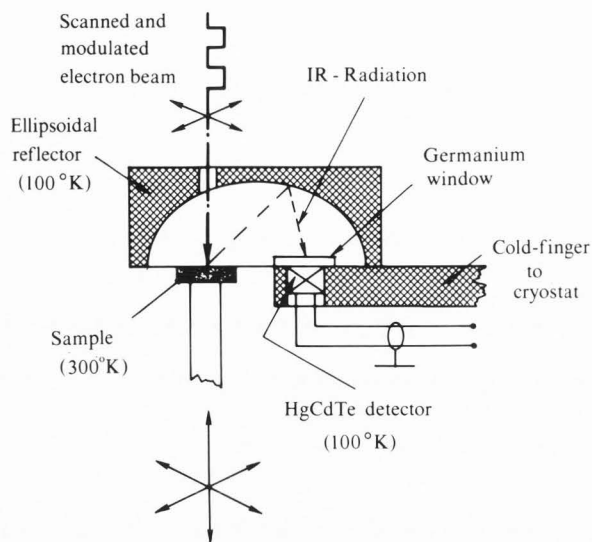Fig. 1 Sample configuration and chopped electron beam scanning mode.

Fig. 2 Detection system with ellipsoidal reflector and infrared detector at 100°K, and sample at room temperature.
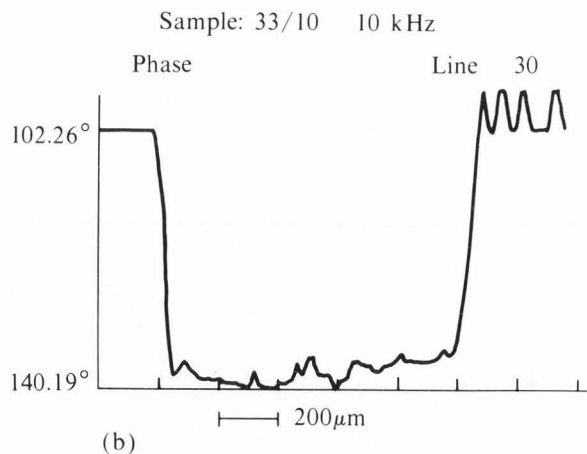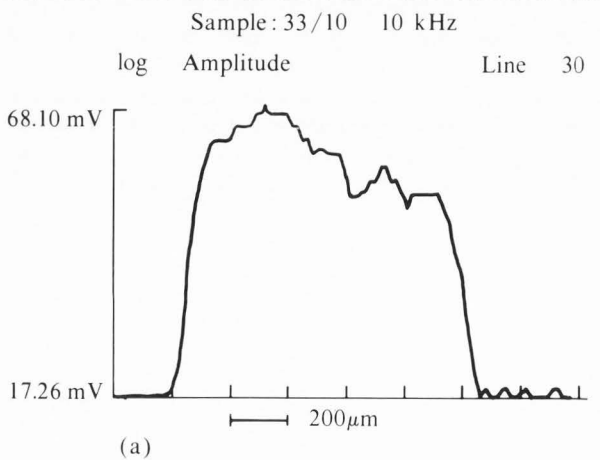
Sample : 33/10   10 kHz

log   Amplitude   Line   30

68.10 mV

17.26 mV

⊢——⊣ 200μm

(a)

Sample: 33/10   10 kHz

Phase   Line   30

102.26°

140.19°

⊢——⊣ 200μm

(b)

Fig. 4 A line scan a) of log amplitude and b) the phase information of the image shown in Fig. 3.

Sample : 33/10   10 kHz

log   Amplitude   Phase
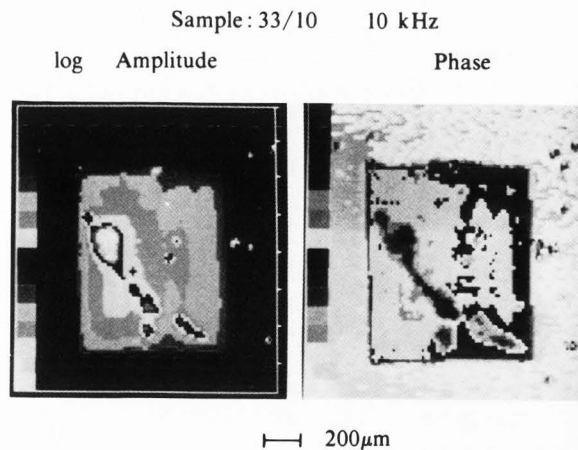

⊢——⊣ 200μm

Fig. 3 Scanned thermal images of sample described in Fig. 1 at 10 kHz modulation frequency and 10⁴ cycles per pixel, 103 × 87 pixels per frame. Scanning time 7.46 minutes. (Black and white copy of color monitor; scale at left.)
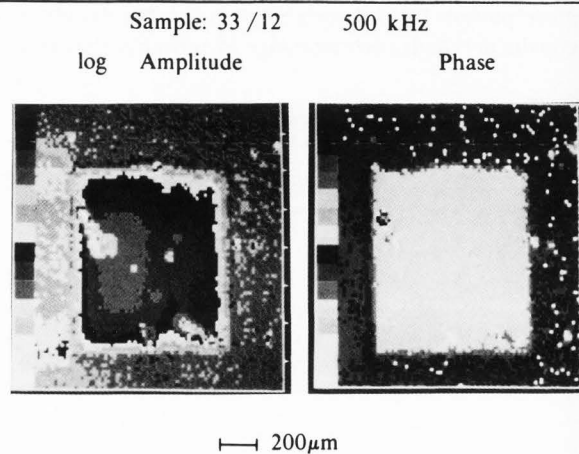
Sample: 33/12   500 kHz

log   Amplitude   Phase

⊢——⊣ 200μm

Fig. 5 Same as Fig. 3, except that modulation frequency is 500 kHz and 2 × 10⁴ cycles per pixel, 103 × 87 pixels per frame. Scanning time 5.97 minutes. (Black and white copy of color monitor; scale at left.)

of a 0.2 mm thick silicon wafer with 2000Å Si_3N_4 grown on one surface. A window of about 1 mm square was then etched out of the opposite side of the silicon wafer without affecting the Si_3N_4 layer. On top of the silicon nitride, a layer of 2000Å gold was evaporated to provide a ground path for the electrons.

As the electron beam heats the surface, a thermal wave propagates inside the sample. This wave and any reflected waves from inhomogeneities in the sample will produce a characteristic temperature profile on the sample surface. The infrared radiation from this surface temperature profile is detected by an infrared detector.[7]

In our configuration, the collection of the infrared radiation is achieved by an aluminum ellipsoidal reflector

with the sample and detector positioned at the focal points of the ellipsoid as shown in Fig. 2. The assembly of reflector and detector are connected via a coldfinger to a cryostat which permits cooling of both to 100°K. Through an entrance hole above the sample focal point, the electron beam enters the ellipsoidal reflector. A grounded germanium window prevents stray electrons and visible radiation from reaching the detector. The sample is maintained at room temperature.

The resolution of our system is not governed by the ellipsoidal reflector, but rather by the beam size (radius a), sample geometry and thermal diffusion length $1_{diff} \equiv (2\kappa/\omega_0)^{1/2}$ where κ is diffusivity and $f_0 = \omega_0/2\pi$ the frequency. ($1_{diff} \sim 3\mu m$ for $\kappa \sim 10^{-2}cm^2/v_s$ and $f_0 \sim 10^5$ Hz). Inhomogeneities at a distance d_s from the heated spot $d_s >> 1_{diff}$ do not contribute significantly to the infrared signal. The sample area to be scanned is divided into 512×512 pixels, which is constant throughout the magnification range of the electron microscope. There is a one-to-one relationship between the heated area and the detected infrared signal.

In our experiments, we used the electron beam of a Cambridge Instrument Mark II A scanning electron microscope, focused to about one square micrometer. The beam power absorbed by the sample was about 2 mW at 20 kV accelerating voltage. The infrared detector was a HgCdTe photoconductor (supplied by the Santa Barbara Research Center) cooled to 100° K. It had a sensitive area of 2mm × 2mm. The detector responsivity (at λ_{max} and at 10 k Hz) is 2×10^2V/W and the detectivity D* (λ_{max} and 10 k Hz) is 2×10^{10}cmHz$^{1/2}$/W. The detector is used in conjunction with a Santa Barbara Research Center amplifier A110 which has a voltage gain of $\approx$ 80 db (unterminated). The detector output is applied to a lock-in amplifier used as a narrow-band receiver, with both in-phase and quadrature channels. An IBM Personal computer controlled the modulation and scanning of the electron beam, and, in addition, collected, stored, processed, and displayed the thermal images. The images are displayed using 16 colors or grey levels. At a modulation frequency of 10 kHz, the thermal images obtained from the sample described above and in Fig. 1 are shown in Fig. 3. The etched window, not visible optically, is shown with good contrast. Window contrast inhomogeneities are due to variations in silicon nitride film thickness and surface contamination. The thermally imaged area is about 1.5 × 1.3mm and consists of 103×87 pixels. A scan of one line of the image is shown in Fig. 4.

The phase difference (Fig. 4b) at $f_0 = 10$kHz between the window (140°) and the bulk silicon wafer $\sim 102°$ is $\sim 38°$. This phase difference is in reasonable agreement with a calculated difference of 45° between a thermally thin and a thermally thick sample.

At higher modulation frequencies (e.g. 500 kHz) similar results are obtained as shown in Fig. 5. The thermal contrast is somewhat less. This is in part due to a dropoff in detector and amplifier performance and in part

due to the $f_0^{-1/2}$ dependence of the thermal signal for a thermally thick sample and f_0^{-1} for a thermally thin sample.

Theory

To analyze the thermal wave imaging system, we follow the square wave modulated electron beam of frequency $\omega_0 = 2\pi f_0$ and its associated time dependent power P(t). Heating the surface at a point (electron beam area $\approx 1\mu m^2$) with coordinates of x_p, y_p, gives rise via the heat diffusion equation to a time dependent temperature distribution in the vicinity of this point of

$$T(t, x_p, y_p, x, y, z) = T_0 + \Delta T(x_p, y_p, x, y, z)$$
$$+ \sum_{n=1,3,5...}^{\infty} T_n(x_p, y_p, x, y, z) \exp(jn\omega_0 t)$$

(1)

with T_0 being the ambient room temperature. ΔT is the DC-temperature distribution due to the DC-component of P(t). The amplitudes of odd harmonic frequency components of temperature are T_n. By employing a narrowband phase-sensitive receiving system, we only measure the ω_0 frequency component, I_1, of the infrared signal. I_1 is calculated with a linearized approximation of the Stefan-Boltzmann Law for black body radiation.

$$I_1(x_p, y_p) \approx 4\sigma T_0^2 \int_{-\infty}^{+\infty} \int_{-\infty}^{+\infty} \varepsilon \left[T_0 + 3\Delta T(x_p, y_p, x, y, z = 0) \right]$$
$$\times T_1(x_p, y_p, x, y, z = 0) \ dx \ dy .$$

(2)

Here, σ is the Stefan-Boltzmann constant and $\varepsilon = \varepsilon(x,y)$, the emissivity of the sample surface. In the stepwise scanning mode, a matrix $I_1(x_p, y_p)$ is recorded. The two components of $I_1(x_p, y_p)$ (i.e., the in-phase and quadrature signals) are recorded and allow the reconstruction of either a "phase" or an "amplitude" digital image. The signal detected is due to pure infrared emission from the sample and hence is purely thermal. Thermal wave imaging systems which use piezoelectric detectors are actually detecting acoustic waves. Therefore, the image contrast can arise from either thermal or elastic inhomogeneities or both.

Conclusion

The above results demonstrate that non-contact thermal imaging of subsurface features can be achieved using a scanned, modulated energy source together with infrared detection. Operation at frequencies to 500 kHz using a cooled IR detector is reported. Further improvement in detector sensitivity and lower detector noise are expected. A direct comparison to a thermoacoustic detection system is presently not possible.

Dacol, F. H., Ermert, H., Melcher, R. L.

References

1. Baumann T, Dacol FH, Melcher RL. (1983). Transmission thermal-wave microscopy with pyroelectric detection. Appl. Phys. Lett. *43*, 71-73.

2. Brandis E, Rosencwaig A. (1980). Thermal-wave microscopy with electron beams. Appl. Phys. Lett. *37*, 98-100.

3. Busse G, Renk KF. (1983). Stereoscopic depth analysis by thermal wave transmission for nondestructive evaluation. Appl. Phys. Lett. *42*, 366-368.

4. Busse G, Eyerer P. (1983). Thermal wave remote and nondestructive inspection of polymers. Appl. Phys. Lett. *43*, 355-357.

5. Busse G. (1983). Optically generated thermal waves for non-destructive material probing and imaging. Journal de Physique *44*, C6, Suppl. au No. 10, 427-436.

6. Cargill III GS. (1980). Ultrasonic imaging in scanning electron microscopy. Nature *286*, 691-693.

7. Ermert H, Dacol FH, Melcher RL, Baumann T. (1984). Noncontact thermal-wave imaging of subsurface structure with infrared detection. Appl. Phys. Lett. *44*, 1136-1138.

8. Fournier D, Bocarra AC. (1980). The mirage effect in photothermal imaging. Scanned Image Microscopy, edited by Ash EA, Academic London, 347-351.

9. Jackson W, Amer NM. (1980). Piezoelectric photoacoustic detection: Theory and experiment. J. Appl. Phys. *51*, 3343-3353.

10. Kolodner P, Tyson JA. (1983). Remote thermal imaging with 0.7μm spatial resolution using temperature-dependent fluorescent thin films. Appl. Phys. Lett. *42*, 117-119.

11. Luukkala M, Lehto A, Jaarinen J, Jokinen M. (1983). Photothermal imaging and thermal surface waves as a NDT tool for coating. 1982 Ultrasonics Symposium Proceedings, Vol. 2, IEEE Cat. No. 82Ch1823-4, 591-594.

12. Nordal PE, Kanstad SO. (1980). Photothermal radiometry for spatial mapping of spectral and material properties. Scanned Image Microscopy, edited by Ash EA (Academic London), 331-339.

13. Rosencwaig A, Opsal J, Willenborg DL. (1983). Thin-film thickness measurements with thermal waves. Appl. Phys. Lett. *43*, 166-168.

14. Thomas RL, Pouch JJ, Wong YH, Favro LD, Kuo PK, Rosencwaig A. (1980). Subsurface flaw detection in metals by photoacoustic microscopy. J. Appl. Phys. *51*, 1152-1156.

Editor's Note: All of the reviewers' concerns were appropriately addressed by text changes, hence there is no Discussion with Reviewers.